SCALING OF DRAG REDUCTION IN A TURBULENT BOUNDARY LAYER BASED ON PLASMA-GENERATED STREAMWISE VORTICES

Xiaohui Wei
Center for Turbulence Control
Harbin Institute of Technology (Shenzhen)
Shenzhen 518055, China
weixiaohui17@mails.ucas.edu.cn

Yu Zhou*
Center for Turbulence Control
Harbin Institute of Technology (Shenzhen)
Shenzhen 518055, China
yuzhou@hit.edu.cn
*Corresponding author

ABSTRACT

Skin-friction drag reduction (DR) in a turbulent boundary layer (TBL) using plasma-generated streamwise vortices (PGSVs) is governed by plasma-induced spanwise wall-jet velocity W, the distance L between the positive electrodes of two adjacent plasma actuators (PAs) or one pair of PAs, and the friction Rynolds number Re_τ. It is experimentally found that DR increases logarithmically with the growing maximum spanwise mean velocity $\overline{W}^+_{max}$ but decreases with rising L^+ and Re_τ, where superscript + denotes normalization by the inner scales. It is further found from theoretical and empirical scaling analysis that the dimensionless drag variation $\Delta F = f_1(\overline{W}^+_{max}, L^+, Re_\tau)$ may be reduced to $\Delta F = f_2(\Gamma)$, where f_1 and f_2 are different functions and the scaling factor $\Gamma = [k_2\log_{10}(k_1 \overline{W}^+_{max})]/(L^+Re_\tau)$ (k_2 and k_1 are constants) is physically the circulation of PGSV. Discussion is conducted based on $\Delta F = f_2(\Gamma)$, which provides important insight into the TBL control physics.

1 INTRODUCTION

Investigations on skin-friction drag reduction (DR) in the turbulent boundary layer (TBL) has been extensively pursued since the late 1970s (Kline *et al*. 1967) due to its potential benefits in various engineering applications, particularly in aeronautics. One of the most popular approaches in this field is the dielectric barrier discharge (DBD) plasma actuator (PA). Cheng *et al*. (2021) and Thomas *et al*. (2019) are perhaps the latest two representative experimental investigations. The former studied three configurations of PA arrays that can generated counter- or co-rotating large-scale streamwise vortices, achieving at the friction Reynolds number $Re_\tau = 572$ a maximum spatially averaged DR of 26% downstream of the actuators. However, the DR on the region where the PA array was placed could not be measured in their work because of the limitations of the actuators' lifespan and force balance's thermal and electrical isolations. Thomas *et al*. (2019) investigated two configurations of PA arrays that could generate counter- and co-rotating large-scale streamwise vortices, respectively, and obtained a spatially averaged DR over the actuation region in excess of 70% at the momentim Reynolds number $Re_\theta = 4538 \sim 18500$. They performed a quantitative analysis of the DR as the function of a single parameter, i.e., the plasma-induced maximum spanwise mean velocity $\overline{W}^+_{max}$ or the distance L^+ between the positive electrodes of two adjacent PAs, for the co-rotating PA array, though the interplay among Re_θ, $\overline{W}^+_{max}$ and L^+ was not studied. This study aims to address these issues.

This work presents an experimental investigation on DR following Cheng *et al.* (2021) and the analysis of available data produced from PGSVs in the literature, focusing on the interrelationships between Re_τ, $\overline{W}^+_{max}$ and L^+. The experimental set-up is similar to that used by Cheng *et al.* (2021*b*). However, with the material of dielectric panel replaced by mica paper, the PA has been significantly improved in terms of its lifespan. So has the force balance deployed, with an anti-static Bakelite plate as its FE which provides a greatly enhanced thermal and electrical isolation from PA array. As such, the spatial averaged DR on the actuation region may be captured directly by the balance, and the PA array may be continuously used at applied voltage $E_{p\text{-}p} = 1.2 \sim 6.0$ $kV_{p\text{-}p}$ (subscript p-p denotes peak-to-peak) and $Re_\tau = 564 \sim 811$.

The paper is organized as following. Experimental details are provided in § 2. The DR results and particle image velocimetry (PIV) measurements are presented in § 3, with a focus on the dependence of DR on individual control parameters. § 4 presents a scaling law for the DR and inferences from this law. This work is summarized and concluded in § 5.

2 EXPERIMENTAL DETAILS

The setup of generation of fully developed TBL is the same as that mentioned in Cheng et al. (2021) and (Qiao, Zhou & Wu 2017) (figure 1*a*). The characteristic parameters of the TBL at various free-stream velocities ranging from 2.4 to 5.0 m/s are presented in table 1 which includes the TBL thickness δ, friction velocity u_τ, viscous length scale $\delta_v = \nu / u_\tau$, and Re_τ based on u_τ. Unless otherwise stated, the superscript '+' in this paper denote normalization by the inner scales in the absence of control. The coordinate system (x, y, z) is defined in figure 1, with the origin at the mid-point of the trailing edge of the PA array. The instantaneous velocities along the x, y and z directions are denoted by U, V and W, respectively.

Table 1. Characteristic parameters of the TBL.

U_∞ (m/s)	δ (mm)	Re_τ	u_τ (m/s)	δ_v (mm)
2.4	80	520	0.102	0.154
3.0	70	564	0.127	0.124
3.6	67	609	0.142	0.110
4.3	64	683	0.170	0.092
5.0	63	747	0.186	0.084

The present PA configuration (Figure 1*b* and *c*) is the same as configuration B in Cheng *et al.* (2021), though 0.2mm-thick mica paper is used as the dielectric material to replace their Mylar and Kapton tapes, which acts to prolong greatly the lifespan of PA. The PA is placed on the FE (210 mm × 240 mm) of our newly improved force balance where the load cell is well isolated from the thermal and electrical effects associated with PA. As a result, the variation in DR on the FE may be captured in real time. A plasma-induced wall jet is generated from the upper to the lower electrode using a sinusoidal alternative current waveform applied with a voltage E_{p-p} = 1.2 ~ 6.0 kV_{p-p} (subscript p-p denotes peak-to-peak). The frequency of E is fixed at 11 kHz.

The high-resolution FE force balance proposed in Cheng *et al.* (2021) has a significant improvement in current measurements (figure 1*a*). The material of FE has been changed from a 1 mm carbon fiber plate to a 2 mm anti-static Bakelite plate with its electric resistance range of 10^8 to 10^{10} Ω. This anti-static Bakelite plate is connected to the ground without tension through a copper foil with a width of 5 mm and a thickness of 0.05 mm, which can shield the electromagnetic and thermal interference generated by plasma and protect the measurements of the load cell. The force balance is calibrated using the skin-friction drag on the FE measured over a range of U_∞, which is proposed by Cheng *et al.* (2021). The drag variation caused by PGSVs under identical experimental conditions is assessed through twelve repeated measurements to determine the mean value. Note that each individual measurement lasts for 30 seconds, following a 60-second operation of the PA array, allowing for the measurement of drag variation during the steady state of PA's discharge.

A Dantec time-resolved PIV system is used to measure the structure of plasma-generated streamwise vortices (PGSVs) in *y-z* plane of x = -105 mm at U_∞ = 2.4, 3.6 and 5.0 m/s. The flow is illuminated by 3.0 mm thick laser sheets shining through the side window, produced by a dual beam laser system (Beamtech Vlite-200, with a maximum frequency and pulse energy of 15 Hz and 200 mJ, respectively) in conjunction with spherical and cylindrical lenses. A high-quality mirror of 80 mm×150 mm is fixed on the plate at x=0.51 m, 45 ° with respect to the *y-z* plane, downstream of the plasma actuator so that the images in the plane could be captured by a high-speed camera (Imager pro HS4M, 4-megapixel sensors, 2016 × 2016 pixels resolution) placed outside the working section. The image covers an area of 80 mm × 80 mm. The total number of images captured is 2000 pairs for measurement with a sampling frequency of 15 Hz.

3 EXPERIMENTAL RESULTS

3.1 Dependence of DR on every single parameter

The newly improved FE force balance is used to accurately measure the DR by capturing the spatially averaged drag variation within the region of the PA array (figure 1*a*). The control performance is evaluated through the drag variation $\Delta F = (F_{on} - F_{off})/F_{off}$, where F_{on} and F_{off} are skin-friction drag acting on the FE with and without control, respectively. The ΔF depends on the on the E_{p-p} imposed as well as on the Re_τ, as shown in figure 2(*a*), where the dashed line is a cubic polynomial fit to the data. In general, ΔF dips with increasing E_{p-p} for Re_τ = 564 ~ 811, as noted by Cheng *et al.* (2021) and Thomas *et al.* (2019). With increasing E_{p-p}, the PGSVs and their associated spanwise wall jets are strengthened (Jukes *et al*. 2006), resulting in a more pronounced DR (Yao *et al*. 2018). The maximum DR of all Reynolds numbers occurs at E_{p-p} = 5.6 ~ 6.0 kV_{p-p}, which is well agree with the E_{p-p} = 5.75 kV_{p-p} at the occurrence of the maximum DR in Cheng *et al.* (2021). However, ΔF increases or DR decreases with increasing Re_τ, from 70% at Re_τ = 564 to only 18% at Re_τ = 811. This drop is attributed to the relatively weakened strength of PGSVs at higher Re_τ compared to their lower Re_τ counterparts, which will be discussed detailly in § 3.2. Evidently, ΔF exhibits a logarithmic decrease with increasing the maximum plasma-induced spanwise wall-jet mean velocity $\overline{W}^+_{max}$ for a given Re_τ, as shown in figure 2(*b*). This finding stands in stark contrast to the results reported by Thomas *et al.* (2019). Thomas *et al.* (2019) observed a linear relationship between ΔF and $\overline{W}^+_{max}$ for the co-rotating streamwise vortices PA array over the range of Re_θ = 4538 ~ 11636. However, note that the range of $\overline{W}^+_{max}$ considered in Thomas *et al.* (2019) was relatively small, ranging from 0.4 to 1.6, which is significantly narrower compared to the broader range of $\overline{W}^+_{max}$ in the present study, spanning from 0.01 to 6.87. Hence, the logarithmic decrease of ΔF with increasing $\overline{W}^+_{max}$ observed in this study can be attributed to the wider range of $\overline{W}^+_{max}$ examined, as opposed to the linear relationship reported by Thomas et al. (2019).

The ΔF exhibits further dependences on L^+ and Re_τ are shown in figure 2(*c*) and (*d*), respectively. In general, ΔF increases or DR decreases with the increasing $L^+$for a given $\overline{W}_{max}$, as observed in both the present investigation and Thomas *et al*.'s (2019) investigation, which indicates that this trend is not unique to any particular configuration of the PA array. Considering Re_τ as $\delta^+ = \delta / \delta_\nu$, where δ^+ is the boundary layer disturbance thickness, the units of Re_τ and L^+ are the same. Therefore, the dependence of ΔF on L^+ and Re_τ exhibits a similar tendency, indicating a consistent relationship between both parameters.

3.2 Plasma-induced flow structure and vorticity circulation

One pair of counter-rotating streamwise vortices is generated by each PA, as is evident in the PIV images (figure 3) captured at the center of PA array, i.e. x = -105 mm, covering a range of -32 mm ≤ z ≤32 mm. The applied voltage on PA array is 6.0 kV_{p-p}. At Re_τ = 564 or x^+ = -741, the maximum vorticity $|\overline{\omega^+_x}|_{max}$ PGSVs normalization by the inner scales, is approximately 0.42 as shown in figure 3(*a*). However, at Re_τ = 685 or x^+ = -1032 and Re_τ = 811 or x^+ = -1352, the corresponding values are only 0.24 (figure 3*b*) and 0.18 (figure 3*c*), respectively. These results suggest that the strength of PGSVs weakens with increasing Re_τ and this reduction in strength is further demonstrated in figure 2(*a*) and (*b*), where the DR decreases. On the other hand, as Re_τ increases, the area covered by PGSVs remains almost constant, forming a circle with an inner-scale normalized diameter of $d^+ \approx 50$ as demonstrated in figure 3, while the cross-sectional area ($L^+ \times Re_\tau$) of the TBL gradually increases. Therefore, the relative area affected by PGSVs compared to the cross-sectional area of the TBL becomes smaller at a higher L^+ or Re_τ, which also diminishes the effect of PGSVs. This adverse effect contributes to the decrease of DR illustrated in figure 2(*c*) and (*d*).

Both the strength and affected area of PGSVs can be simultaneously quantified by evaluating the inner-scale vorticity circulation Γ^+ over a specific area. This area is defined by the condition $|\overline{\omega^+_x}| > r|\overline{\omega^+_x}|_{max}$, where r is a constant within the range of 0 to 1. The boundary vorticity flux $\boldsymbol{\sigma} = \nu\boldsymbol{n}\times(\nabla\times\boldsymbol{\omega})$ (Lyman 1990 and Terrington, Hourigan & Thompson 2022) can be simplified to $\sigma' = |\nabla\times\boldsymbol{\omega}|$ in the present study, where $\boldsymbol{n}$ is the outward-directed unit normal to the control-volume boundary, ∇ is the differential operator and vorticity vector $\boldsymbol{\omega} = [\omega_x, \omega_y, \omega_z] = [|\overline{\omega_x^+}|, 0, 0]$ in the present study. Applying this formulation to discrete experimental data with a chosen value of r = 0.8, the vorticity circulation is calculated as the sum of σ' over an area where $|\overline{\omega_x^+}| > 0.8|\overline{\omega_x^+}|_{max}$, i.e. $\Gamma^+_{0.8} = \sum \sigma'_{0.8}$, where subscribe 0.8 denote r. The equation clearly shows that $\Gamma^+_{0.8}$ increases with increasing $|\overline{\omega_x^+}|$ which represents the strength of the PGSV measured using PIV at E_{p-p} = 6.0 kV_{p-p} (figure 3). The calculated results of $\Gamma^+_{0.8}$ are 1.604 with a DR of 70%, 0.988 with a DR of 32% and 0.657 with a DR of 18% at Re_τ = 564, 685 and 811, respectively, indicating a direct and positive relationship between the PGSVs-induced DR and Γ^+.

4 DISCUSSION

4.1 A scaling law for the DR

The figure 2 evidently illustrates that ΔF depends on three parameters, viz. $\Delta F = f_1\,(\overline{W}^+_{max}, L^+, Re_\tau)$. Careful theoretical and experimental data analyses along with numerous trial-and-error attempts unveil that the data of ΔF collapse well around one single curve once $\Gamma_{W,\,L,\,Re} = [k_2\log_{10}(k_1\overline{W}^+_{max})]/(L^+\delta^+)$ is used as the abscissa, where k_1 and k_2 are parameters that depends on the curve fitting process (figure 4). In the present study, the results demonstrate that $k_1 = 10^3$ and $k_2 \approx 1$. The obtained results show a strong collapse, and thus it could be concluded that it is crucial to account for the interaction of these three parameters. Therefore, $\Delta F = f_1\,(\overline{W}^+_{max}, L^+, Re_\tau)$ is now reduced to $\Delta F = f_2\,(\Gamma_{W,\,L,\,Re}) \approx -3.8\times10^4\Gamma_{W,\,L,\,Re}$, where both ΔF and $\Gamma_{W,\,L,\,Re}$ are dimensionless and the negative sign means a drag reduction since $\Gamma_{W,\,L,\,Re}$ is always positive. Clearly, ΔF drops or DR increases almost linearly with growing $\Gamma_{W,\,L,\,Re}$. Note that the Re_τ effect is embedded in $\overline{W}^+_{max}$, L^+ and δ^+ because the three parameters are all non-dimensionalized by u_τ or δ_v that are directly related to Re_τ. To understand the scaling law $\Delta F = f_2\,(\Gamma_{W,\,L,\,Re})$ or the physical meaning of the scaling factor $\Gamma_{W,\,L,\,Re}$, we consider the vorticity circulation $\Gamma^+_{0.8}$ whose border is defined at $|\overline{\omega_x^+}| = 0.8|\overline{\omega_x^+}|_{max}$ as mentioned earlier. Note that $\Gamma^+_{0.8}$ is measured at E_{p-p} = 6.0 kV_{p-p} and at Re_τ = 564, 658 and 811. When the value of $\Gamma^+_{0.8}$ is scaled down by a factor of 10^5, i.e. $10^{-5}\Gamma^+_{0.8}$, it is surprisingly found that $10^{-5}\Gamma^+_{0.8}$ measured by PIV aligns well with the results obtained from the high-resolution FE force balance (figure 4). Consequently, $\Delta F = f_1\,(\overline{W}^+_{max}, L^+, Re_\tau)$ can be also reduced to $\Delta F = f_2\,(10^{-5}\Gamma^+_{0.8}) \approx -3.8\times10^4(10^{-5}\Gamma^+_{0.8})$. This agreement between the PIV and high-resolution FE force balance measurements further supports the validity and accuracy of the scaling factor utilized in the analysis. The results suggest that the DR scales with the vorticity circulation of PGSV.

4.2 Inferences from the scaling law

The scaling law reveals some interesting inferences. Firstly, given two of the parameters $\overline{W}^+_{max}$, L^+ and Re_τ, the effect of the remaining parameter on ΔF may be determined from the scaling law. For example, in figure 5(a), given L^+ = 500 and Re_τ = 700, ΔF decreases or DR increases with increasing $\overline{W}^+_{max}$. Secondly, when $\Gamma_{W,\,L,\,Re}$ or ΔF is given, as the production of L^+ and δ^+ decreases, $\overline{W}^+_{max}$ also decreases, making the less energy consumption of PA and thus increasing efficiency. Figure 5(b) shows the contour map of dependence of ΔF on $\overline{W}^+_{max}$ and $L^+\delta^+$. The blackbody cross symbols are control efficiency $\eta = (F_{on} - F_{off})U_\infty/P_{input}$, where P_{input} is the power consumption determined by Q-V cycloramas (Lissajous figures) measured through two parallel- and series-connected capacitances at $\Delta F \approx -0.185$. As illustrated in Figure 5(b), η decreases with the decreasing $L^+\delta^+$ and $\overline{W}^+_{max}$. Thirdly, due to the similarity between L^+ and Re_τ (figure 2c and d), the scaling law factor $\Gamma_{W,\,L,\,Re}$ can be further simplified to $\Gamma_{W,\,L} = [k_2\log_{10}(k_1\overline{W}^+_{max})]/L^+$ by omitting Re_τ, i.e. δ^+ (figure 5c). Then the k_1 and k_2 are 10^4 and 1, respectively. These values are also determined through a curve fitting process. The fitted curve function is $\Delta F \approx -4300\Gamma_{W,\,L}^2 - 6.3\Gamma_{W,\,L} - 0.02$. Note that $10^{-5}\Gamma^+_{0.8}$ in figure 4 is now $10^{-2}\Gamma^+_{0.83}$ in figure 5(c), where $\Gamma^+_{0.83}$ is vorticity circulation whose border is defined at $|\overline{\omega_x^+}| = 0.83|\overline{\omega_x^+}|_{max}$, which furtherly demonstrate s that the DR scales with the vorticity circulation of PGSV despite the scaling law factor of $\Gamma_{W,\,L}$. Both figure 4 and figure 5(c) show that the proposed scaling law for the DR can effectively encompass the experimental data, demonstrating high reliability and robustness. Lastly, once $\Gamma_{W,\,L,\,Re}$ or $\Gamma_{W,\,L}$ is known, DR can be predicted, providing a theoretical basis for the design of PA arrays.

5 CONCLUSIONS

A TBL at Re_τ = 564 ~ 811 are experimentally manipulated using a spanwise array of longitudinal dielectric barrier discharge PA with a view to reducing skin friction and investigating the scaling law for control parameters. Following conclusions can be drawn of out this work.

(1) Two parameters, $\overline{W}^+_{max}$ and L^+, of PA array, as well as one parameter, Re_τ, of TBL, have been investigated for reducing the skin-friction drag. The DR logarithmically increases with increasing $\overline{W}^+_{max}$ for a given Re_τ result from the powerful strength of PGSVs at higher $\overline{W}^+_{max}$. This finding differs from the linear relationship reported by Thomas et al. (2019). The discrepancy may be attributed to the wilder range of $\overline{W}^+_{max}$ considered in the present study, which clearly highlights the precise relationship between DR and $\overline{W}^+_{max}$. On the other hand, DR decreases with increasing L^+ or Re_τ because, given the same $\overline{W}_{max}$, the cross-sectional area of TBL expands with increasing L^+ or Re_τ, which relatively reduces the area affected by PGSV.

(2) It has been found for the first time from empirical scaling analysis of obtained experimental data that $\Delta F = f_1\,(\overline{W}^+_{max}, L^+, Re_\tau)$ can be reduced to $\Delta F = f_2\,(\Gamma_{W,\,L,\,Re}) \approx -3.8\times104\Gamma_{W,\,L,\,Re}$. In this function, both ΔF and $\Gamma_{W,\,L,\,Re}$ are dimensionless and the negative sign means a drag reduction since $\Gamma_{W,\,L,\,Re}$ is always positive. The scaling factor $\Gamma_{W,\,L,\,Re} = [k_2\log_{10}(k_1\overline{W}^+_{max})]/(L^+\delta^+)$, where $k_1 = 10^3$ and $k_2 \approx 1$ determined from the curve fitting process. Note that the Re_τ effect is embedded in $\overline{W}^+_{max}$, L^+ and δ^+ because the three parameters are all non-dimensionalized by u_τ or δ_v that are directly related to Re_τ. The PIV measurements demonstrate that $\Delta F = f_1\,(\overline{W}^+_{max}, L^+, Re_\tau)$ can be also reduced to $\Delta F = f_2\,(10^{-5}\Gamma^+_{0.8}) \approx -3.8\times10^4(10^{-5}\Gamma^+_{0.8})$, where $\Gamma^+_{0.8}$ is vorticity circulation whose border is defined at $|\overline{\omega_x^+}| = 0.8|\overline{\omega_x^+}|_{max}$, indicating that the DR scales with the vorticity circulation of PGSV.

(3) Several interesting inferences can be made out of this scaling law. Firstly, given two of the parameters $\overline{W}^+_{max}$, L^+ and Re_τ, the effect of the remaining parameter on ΔF may be determined from the scaling law. Secondly, given $\Gamma_{W,\,L,\,Re}$ or

ΔF, the required $\overline{W}^{+}_{max}$ that is related to the energy consumption of PA drops as the product of L^+ and δ^+ is reduced, that is, the control efficiency improves. Thirdly, due to the similarity between L^+ and Re_τ (figure 2*c* and *d*), the scaling law factor $\Gamma_{W,\,L,\,Re} = [k_2\log_{10}(k_1\overline{W}^{+}_{max})]/(L^+\delta^+)$ can be further simplified to $\Gamma_{W,\,L} = [k_2\log_{10}(k_1\overline{W}^{+}_{max})]/L^+$ by omitting Re_τ, i.e. δ^+ (figure 5*c*). Finally, DR can be predicted once $\Gamma_{W,\,L,\,Re}$ or $\Gamma_{W,\,L}$ is known, which provides a theoretical basis for the design of PA arrays.

ACKNOWLEDGEMENT
YZ wishes to acknowledge support given to him from NSFC through Grant 91952204 and from the Research Grants Council of Shenzhen Government through grant JCYJ20210324132816040.

REFERENCES

Kline, S., Reynolds, W., Schraub, F., & Runstadler, P. 1967 The structure of turbulent boundary layers. *J. Fluid Mech.* **30**, 741-773.

Cheng, X. Q., Wong, C. W., Hussain, F., Schröder, W., & Zhou, Y. 2021 Flat plate drag reduction using plasma-generated streamwise vortices. *J. Fluid Mech.* **918**, A24.

Jukes, T. N., Choi, K.-S., Johnson, G. A. & Scott, S. J. 2006 Characterization of surface plasma-induced wall flows through velocity and temperature measurements. *AIAA J.* **44**, 764–771.

Lyman, F. A. 1990 Vorticity production at a solid boundary. *Appl. Mech. Rev*. **43**, 157-158.

Qiao, Z. X., Zhou, Y. & Wu, Z. 2017 Turbulent boundary layer under the control of different schemes. *Proc. R. Soc. A* 473, 20170038.

Terrington, S., Hourigan, K. & Thompson, M. 2022 Vorticity generation and conservation on generalised interfaces in three-dimensional flows. *J. Fluid Mech.* **936**, A44.

Thomas, F. O., Corke, T. C., Duong, A., Midya, S. & Yates, K. 2019 Turbulent drag reduction using pulsed-DC plasma actuation. *J. Phys. D: Appl. Phys.* **52**, 434001.

Yao, J., Chen, X. & Hussain, F. 2018 Drag control in wall-bounded turbulent flows via spanwise opposed wall-jet forcing. *J. Fluid Mech.* 852, 678–709.

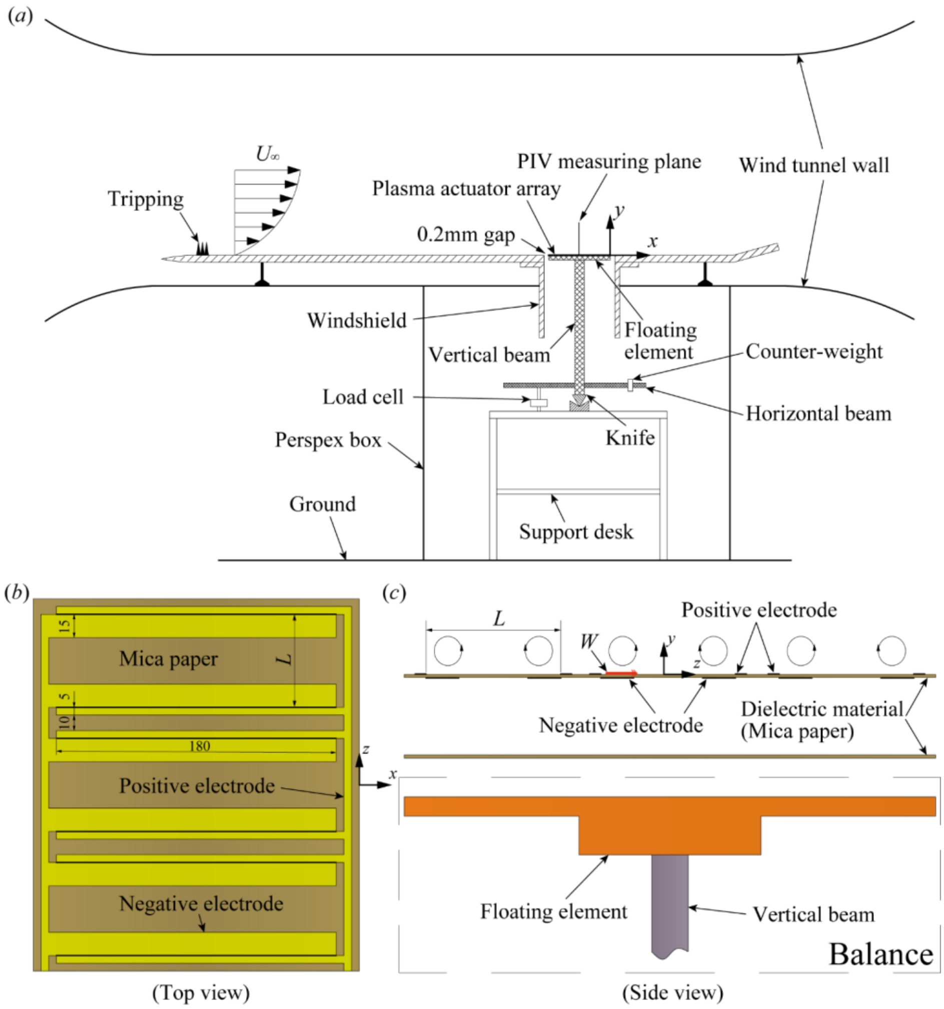

Figure 1. (*a*) Schematic of experimental set-up for the generation of a turbulent boundary layer and the floating-element balance. (*b*) Top and (*c*) side view of schematic of the plasma actuator array (not to scale; dimensions are in millimeters).

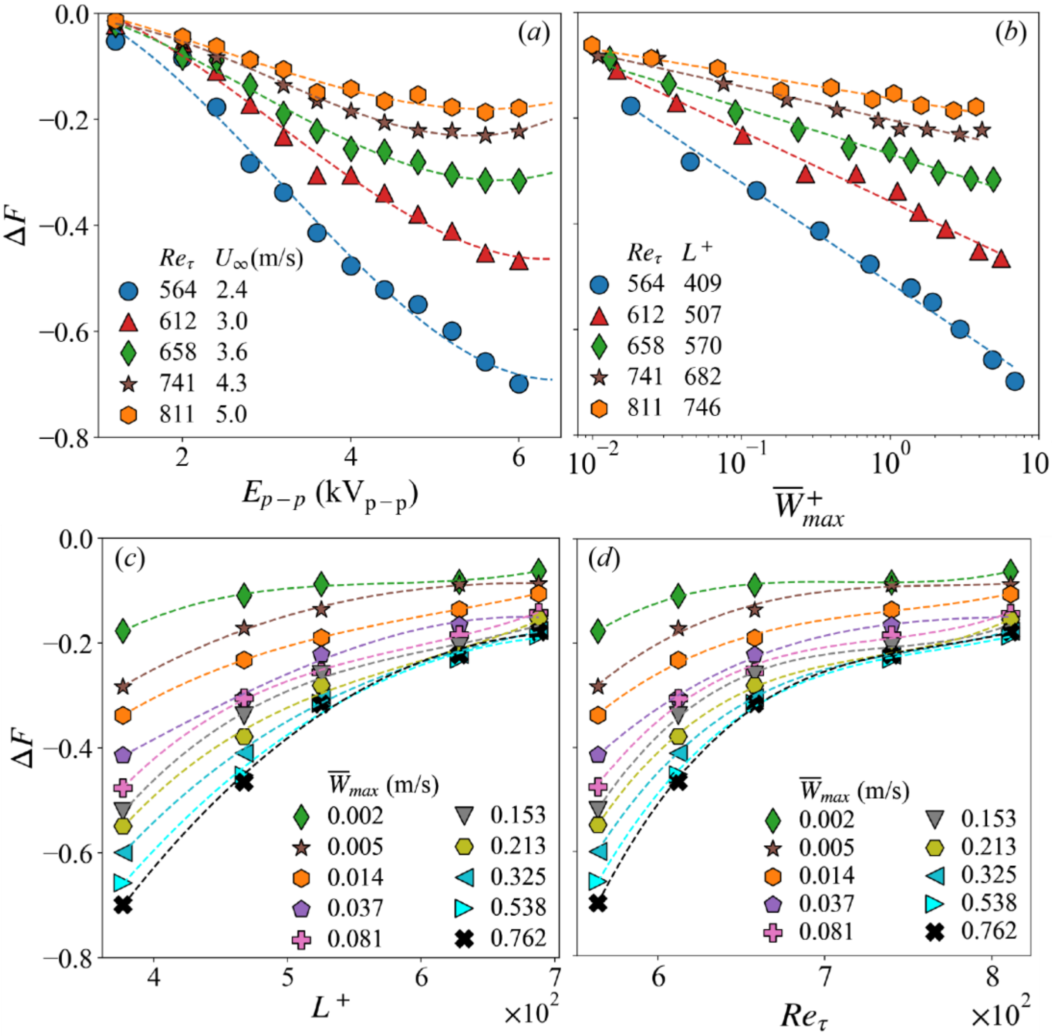

Figure 2. Dependence of drag variation ΔF on (*a*) $E_{p\text{-}p}$, (*b*) $\overline{W}^+_{max}$, (*c*) L^+, and (*d*) Re_τ. Superscript + denotes normalization by the wall unit. The dashed line is a cubic polynomial fit to the data.

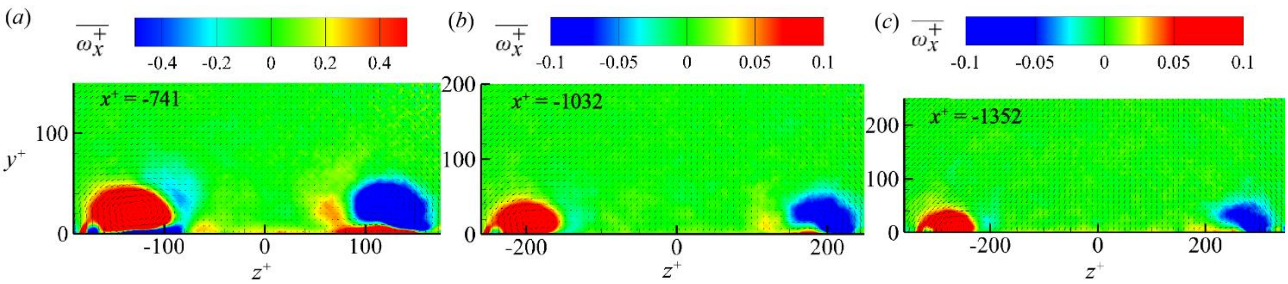

Figure 3. Time-averaged velocity vectors ($\overline{V^+}$, $\overline{W^+}$) and iso-contours of vorticity $\overline{\omega_x^+} = \overline{\mathrm{d}V^+/\mathrm{d}z^+} - \overline{\mathrm{d}W^+/\mathrm{d}y^+}$ in the y-z plane at the center (x = -105 mm) of the PA array. (*a*) Re_τ = 564, (*b*) 658 and (*c*) 811. The applied voltage on plasma actuators is 6.0 $kV_{p\text{-}p}$.

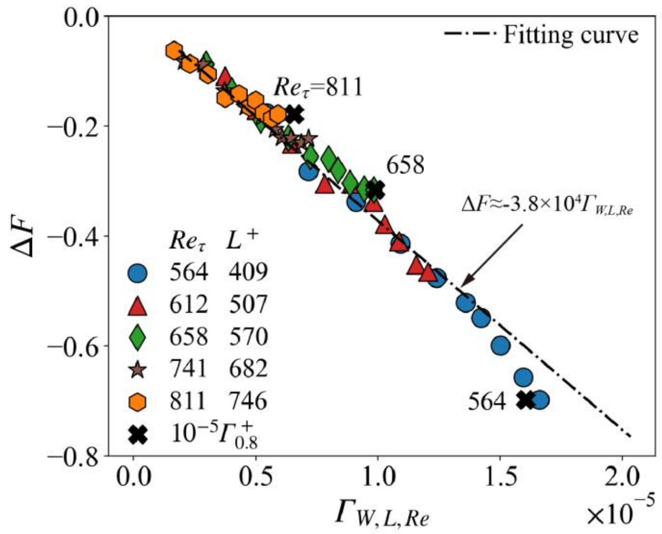

Figure 4. Dependence of drag variation ΔF on $\Gamma_{W,\,L,\,Re}$ = $[k_2\log_{10}(k_1\overline{W}^+_{max})]/L^+\delta^+$, where k_1 = 10^3 and $k_2 \approx 1$. The black cross symbols are 10^{-5} times the measured vorticity circulation $\Gamma^+_{0.8}$ within the PGSV, whose border is defined at $|\overline{\omega^+_x}|$ = $0.8|\overline{\omega^+_x}|_{max}$ ($E_{p\text{-}p}$ = 6 $\mathrm{kV_{p\text{-}p}}$ and Re_τ = 564, 658 and 811). The function of fitting curve is $\Delta F \approx -3.8\times10^4\Gamma_{W,\,L,\,Re}$.

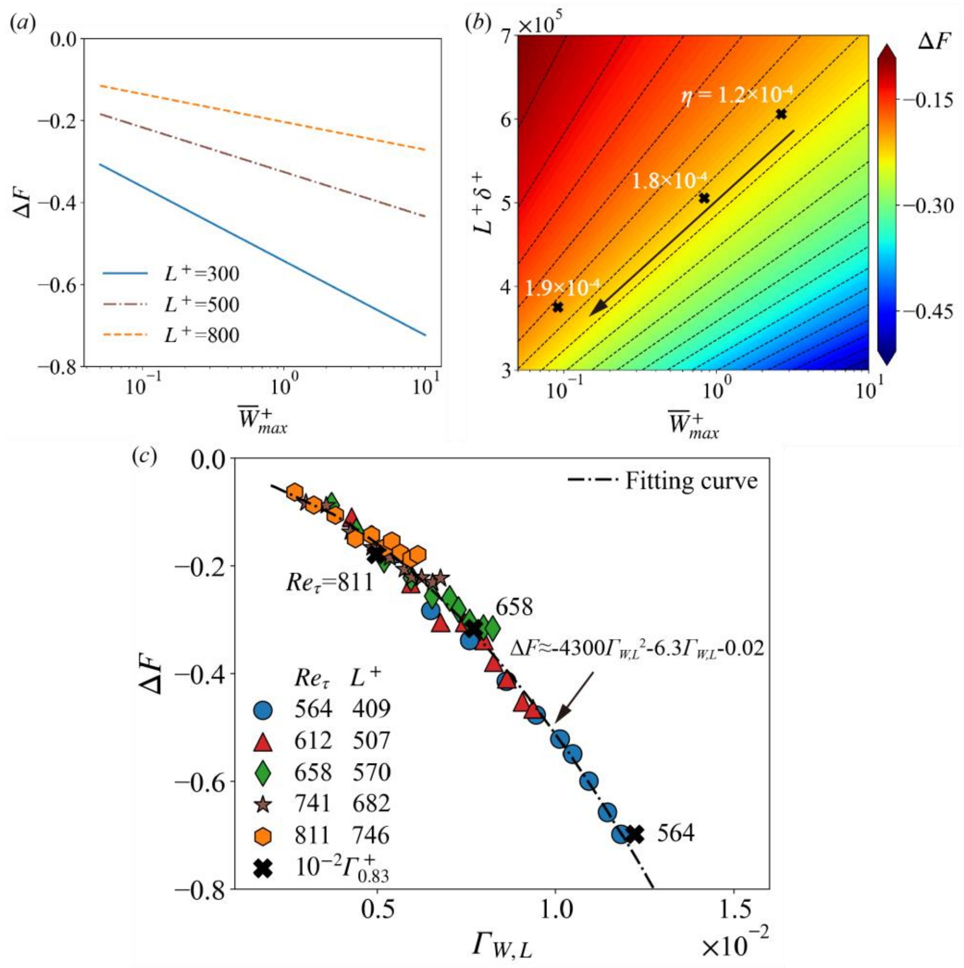

Figure 5. (*a*) Given Re_τ = 700, dependence of ΔF on $\overline{W}^+_{max}$ at L^+ = 300, 500 and 800. (*b*) Contour map of dependence of ΔF on $\overline{W}^+_{max}$ and $L^+\delta^+$. The blackbody cross symbols are control efficiency η measured at $\Delta F \approx -0.185$. Both (*a*) and (*b*) are analyzed based on $\Delta F \approx -3.8\times10^4\Gamma_{W,\,L,\,Re}$. (*c*) Dependence of drag variation ΔF on $\Gamma_{W,\,L}$. The black cross symbols are 10^{-2} times the measured vorticity circulation $\Gamma^+_{0.83}$ within the PGSV, whose border is defined at $|\overline{\omega^+_x}|$ = $0.83|\overline{\omega^+_x}|_{max}$ ($E_{p\text{-}p}$ = 6 $\mathrm{kV_{p\text{-}p}}$ and Re_τ = 564, 658 and 811). The function of fitting curve is $\Delta F \approx -4300\Gamma_{W,\,L}^2-6.3\Gamma_{W,\,L}-0.02$.